

SMEFT predictions for $gg \rightarrow hh$ at full NLO QCD and truncation uncertainties

Gudrun Heinrich,^a Jannis Lang,^a Ludovic Scyboz^b

^a*Institute for Theoretical Physics, Karlsruhe Institute of Technology (KIT), 76131 Karlsruhe, Germany*

^b*Rudolf Peierls Centre for Theoretical Physics, Parks Road, Oxford OX1 3PU, UK*

E-mail: gudrun.heinrich@kit.edu, jannis.lang@kit.edu,
ludovic.scyboz@physics.ox.ac.uk

ABSTRACT: We present a calculation of the NLO QCD corrections for Higgs-boson pair production in gluon fusion including effects of anomalous couplings within Standard Model Effective Field Theory (SMEFT). We study effects of different truncation options of the EFT expansion in $1/\Lambda$ and of double operator insertions, both at total cross-section level as well as for the distribution of the invariant mass of the Higgs-boson pair, at $\sqrt{s} = 13$ TeV. The NLO corrections are implemented in the generator `ggHH.SMEFT` in the `Powheg-Box-V2` framework.

KEYWORDS: LHC, Higgs-boson couplings, NLO, EFT

Contents

1	Introduction	1
2	Description of the EFT framework and the calculation	3
2.1	EFT descriptions of Higgs-boson pair production	3
2.2	Operator insertions at amplitude-squared level	5
3	Implementation and usage of the code within the Powheg-Box	6
3.1	Implementation of the NLO QCD corrections	6
3.2	Usage within the Powheg-Box-V2	7
4	Results	7
4.1	Total cross sections	8
4.2	Distribution of the Higgs-pair invariant mass m_{hh} : truncation effects	11
5	Conclusions	16
6	Addendum	17

1 Introduction

The importance of Higgs-boson pair production as a process allowing us to shed more light on the Higgs potential is undisputed. Deviations from the Standard Model (SM) form, manifesting themselves in anomalous Higgs-boson self-couplings, would be a clear sign of new physics. If the Higgs-boson trilinear coupling was found to be different from the SM value, small deviations in other Higgs couplings could also be expected. In order to expose such slight deviations, it is crucial to control the uncertainties of the theory predictions, including the description of anomalous couplings within an effective field theory (EFT) framework. The theory uncertainties have various sources, the dominant ones in the SM currently being uncertainties related to the treatment of the top-quark mass in different renormalisation schemes. NLO QCD corrections including the full top-quark mass dependence are available [1–4] and have been included in calculations where higher orders have been performed in the heavy-top limit [5–7], thus reducing the scale uncertainties and the uncertainties due to missing top-quark mass effects, while the top-mass scheme uncertainties remain an issue [8].

Going beyond the SM description of the process $gg \rightarrow hh$, effects of anomalous couplings have been studied at NLO in the Born-improved heavy-top limit (HTL) for both CP-conserving [9] as well as CP-violating [10] operators. NLO corrections with full m_t -dependence have been incorporated within a non-linear EFT parametrisation (also called Higgs Effective Field Theory, HEFT) in Ref. [11]. In Ref. [12] the combination of NNLO corrections in the HTL has been performed within the HEFT framework. Finally, in Ref. [13], the full NLO corrections of Ref. [11] have been combined with the NNLO corrections of Ref. [12] to provide approximate NNLO predictions, dubbed NNLO', which include the full top-quark mass dependence up to NLO and higher order corrections up to NNLO in the HTL, combined with operators related to the five most relevant anomalous couplings for the process $gg \rightarrow hh$.

By including the EFT parametrisation of new physics effects into the predictions for Higgs-boson pair production, new uncertainties arise, related to the truncation of the EFT expansion, which relies on an assessment of the relevance of operator contributions to the Lagrangian in a certain well-defined counting scheme. Furthermore, at amplitude squared level, there are several possibilities to truncate the expansion in the canonical dimension, related to the inclusion of squared dimension six terms and double operator insertions. The discussion of truncation uncertainties recently gained considerable attention in the literature [14–22], showing that the uncertainties have to be assessed on a case-by-case basis.

In the following we will present results within SMEFT for Higgs-boson pair production in gluon fusion, including full NLO QCD corrections as well as options to include linear or quadratic terms in the EFT expansion and double operator insertions. This allows us to investigate various scenarios of truncation of the EFT expansion and to assess the related uncertainties compared to the size of the scale uncertainties at NLO QCD. We will also point out differences between a SMEFT and a HEFT description in this context. In section 2, we recap the definition of the SMEFT and HEFT effective field-theory frameworks, specifically of those operators that are of interest for Higgs-pair production, and we outline different ways of defining the truncation at the level of the squared amplitude. In section 3 we give a brief summary of the implementation of the SMEFT predictions at full NLO QCD into the **Powheg-Box-V2** [23–25] event generator. We discuss our results in section 4, and conclude in section 5.

2 Description of the EFT framework and the calculation

2.1 EFT descriptions of Higgs-boson pair production

In this section, we introduce our conventions and contrast the SMEFT and HEFT descriptions at Lagrangian level.

In Standard Model Effective Field Theory (SMEFT) [26–28], a low energy description of unknown interactions at a new physics scale Λ is constructed as an expansion in inverse powers of Λ , with operators \mathcal{O}_i of canonical dimension larger than four and corresponding Wilson coefficients C_i ,

$$\mathcal{L}_{\text{SMEFT}} = \mathcal{L}_{\text{SM}} + \sum_i \frac{C_i^{(6)}}{\Lambda^2} \mathcal{O}_i^{\text{dim6}} + \mathcal{O}\left(\frac{1}{\Lambda^3}\right). \quad (2.1)$$

In SMEFT it is assumed that the physical Higgs boson is part of a doublet transforming linearly under $SU(2)_L \times U(1)$. The SMEFT Lagrangian is usually given in the so-called Warsaw basis [27], where the terms relevant to the process $gg \rightarrow hh$ read

$$\begin{aligned} \Delta\mathcal{L}_{\text{Warsaw}} = & \frac{C_{H,\Box}}{\Lambda^2} (\phi^\dagger \phi) \Box (\phi^\dagger \phi) + \frac{C_{HD}}{\Lambda^2} (\phi^\dagger D_\mu \phi)^* (\phi^\dagger D^\mu \phi) + \frac{C_H}{\Lambda^2} (\phi^\dagger \phi)^3 \\ & + \left(\frac{C_{uH}}{\Lambda^2} \phi^\dagger \phi \bar{q}_L \phi^c t_R + h.c. \right) + \frac{C_{HG}}{\Lambda^2} \phi^\dagger \phi G_{\mu\nu}^a G^{\mu\nu,a}. \end{aligned} \quad (2.2)$$

The dipole operator $\bar{\mathcal{O}}_{uG}$ is not included here because it can be shown that it carries an extra loop suppression factor $1/(4\pi)^2$ relative to the other contributions if weak coupling to the heavy sector is assumed [11, 29, 30]. In the case of a UV completion where the coupling to the heavy sector is strong, SMEFT would not be the appropriate description of the full theory at low energies anyway.

Higgs Effective Field Theory (HEFT) [31–36] instead is based on an expansion in terms of loop orders, which also can be formulated in terms of chiral dimension (d_χ) counting [37–39]. The expansion parameter is given by $f^2/\Lambda^2 \simeq \frac{1}{16\pi^2}$, where f is a typical energy scale at which the EFT expansion is valid (such as the pion decay constant in chiral perturbation theory),

$$\mathcal{L}_{d_\chi} = \mathcal{L}_{(d_\chi=2)} + \sum_{L=1}^{\infty} \sum_i \left(\frac{1}{16\pi^2} \right)^L c_i^{(L)} O_i^{(L)}. \quad (2.3)$$

The HEFT Lagrangian relevant to Higgs-boson pair production in gluon fusion can be parametrised by five a priori independent anomalous couplings as follows [11]

$$\Delta\mathcal{L}_{\text{HEFT}} = -m_t \left(c_t \frac{h}{v} + c_{tt} \frac{h^2}{v^2} \right) \bar{t} t - c_{hhh} \frac{m_h^2}{2v} h^3 + \frac{\alpha_s}{8\pi} \left(c_{ggh} \frac{h}{v} + c_{gghh} \frac{h^2}{v^2} \right) G_{\mu\nu}^a G^{a,\mu\nu}. \quad (2.4)$$

Expanding the Higgs doublet in eq. (2.2) around its vacuum expectation value and applying a field redefinition to the physical Higgs boson

$$h \rightarrow h + v^2 \frac{C_{H,\text{kin}}}{\Lambda^2} \left(h + \frac{h^2}{v} + \frac{h^3}{3v^2} \right), \quad (2.5)$$

with

$$C_{H,\text{kin}} := C_{H,\square} - \frac{1}{4} C_{HD},$$

the Higgs kinetic term acquires its canonical form (up to $\mathcal{O}(\Lambda^{-4})$ terms). After that, the couplings can be related through a comparison of the coefficients of the corresponding terms in the Lagrangian, which leads to the expressions given in Table 1. Note that in the Warsaw basis C_{HG} implicitly contains a factor of α_s relative to c_{ggh} and c_{gghh} and therefore the translation becomes scale-dependent even if no (electroweak) RGE running of the Wilson coefficients is included.

HEFT	Warsaw
c_{hhh}	$1 - 2 \frac{v^2}{\Lambda^2} \frac{v^2}{m_h^2} C_H + 3 \frac{v^2}{\Lambda^2} C_{H,\text{kin}}$
c_t	$1 + \frac{v^2}{\Lambda^2} C_{H,\text{kin}} - \frac{v^2}{\Lambda^2} \frac{v}{\sqrt{2}m_t} C_{uH}$
c_{tt}	$-\frac{v^2}{\Lambda^2} \frac{3v}{2\sqrt{2}m_t} C_{uH} + \frac{v^2}{\Lambda^2} C_{H,\text{kin}}$
c_{ggh}	$\frac{v^2}{\Lambda^2} \frac{8\pi}{\alpha_s} C_{HG}$
c_{gghh}	$\frac{v^2}{\Lambda^2} \frac{4\pi}{\alpha_s} C_{HG}$

Table 1: Translation at Lagrangian level between different operator basis choices.

The translation given in Table 1 suggests that there is no explicit dependence on the scale Λ in the HEFT Wilson coefficients. As mentioned above, the effective HEFT Lagrangian is expanded in powers of $f^2/\Lambda^2 \simeq 1/(4\pi)^2$, with $\Lambda \simeq 4\pi f$ the scale of new physics and f a reference scale for energies where the EFT expansion is valid; for the case of strongly coupled UV completions f corresponds to the scale of dynamical symmetry breaking. In section 4, we will still use the translation for a specific value of the scale Λ to compare SMEFT and HEFT results.

However, it should be pointed out that a translation between the coefficients at Lagrangian level must be applied with care. The EFT parametrisations have a validity range limited by unitarity constraints and the assumption that C_i/Λ^2 in SMEFT is a small quantity. Furthermore, due to different assumptions about the transformation of the Higgs field under the EW symmetry transformations, there are relations between certain coefficients in SMEFT, which are not present in HEFT. Therefore a naive translation from HEFT (which is, in this regard, the more general theory) to SMEFT

can lead out of the validity range of SMEFT for certain points in the coupling parameter space, even though they are perfectly valid points in HEFT.

2.2 Operator insertions at amplitude-squared level

An EFT description is based on an expansion in a parameter encoding the scale hierarchies which underlie the EFT description. Therefore an uncertainty arises due to the truncation of the EFT expansion. In particular, there is the question whether to truncate the SMEFT expansion at amplitude-squared level strictly beyond dimension-6, or to include squared dimension-6 operators, which are of order $1/\Lambda^4$ and therefore formally suppressed at the same order as dimension-8 operators. Furthermore, double operator insertions into a single diagram are usually neglected as they form a subset of operators at order $1/\Lambda^4$ which is not uniquely defined (for example, they can be related to a different set of operators through the equations of motion). Such issues have been discussed recently in Refs. [15, 16, 19–21].

In the next section we present a Monte Carlo program, which includes the full m_t -dependent NLO QCD corrections, and allows the systematic study of truncation effects for the case of Higgs-boson pair production in gluon fusion. In order to construct the different truncation options we divide the amplitude into three parts: the pure SM contribution (SM), single dimension-6 operator insertions (dim6) and double dimension-6 operator insertions (dim6²):

$$\begin{aligned}
\mathcal{M} = & \text{[Diagram 1]} + \text{[Diagram 2]} + \text{[Diagram 3]} \\
& + \text{[Diagram 4]} + \text{[Diagram 5]} + \dots \\
= & \mathcal{M}_{\text{SM}} + \mathcal{M}_{\text{dim6}} + \mathcal{M}_{\text{dim6}^2} , \tag{2.6}
\end{aligned}$$

where C' denotes the corresponding coupling combination listed in Table 1. We consider four possibilities to choose which parts of $|\mathcal{M}|^2$ from eq. (2.6) may enter in the squared

amplitude forming the cross section:

$$\sigma \simeq \begin{cases} \sigma_{\text{SM}} + \sigma_{\text{SM} \times \text{dim}6} & \text{(a)} \\ \sigma_{(\text{SM} + \text{dim}6) \times (\text{SM} + \text{dim}6)} & \text{(b)} \\ \sigma_{(\text{SM} + \text{dim}6) \times (\text{SM} + \text{dim}6)} + \sigma_{\text{SM} \times \text{dim}6^2} & \text{(c)} \\ \sigma_{(\text{SM} + \text{dim}6 + \text{dim}6^2) \times (\text{SM} + \text{dim}6 + \text{dim}6^2)} & \text{(d)} \end{cases} \quad (2.7)$$

Case (a) denotes the first order of an expansion of $\sigma \sim |\mathcal{M}|^2$ in Λ^{-2} , (b) is the first order of an expansion of \mathcal{M} in Λ^{-2} . Case (c) includes all terms of $\mathcal{O}(\Lambda^{-4})$ coming from single and double dimension-6 operator insertions, however it lacks the contribution at the same order from dimension-8 operators and $\mathcal{O}(\Lambda^{-4})$ terms following from the field redefinition of eq. (2.5). Case (d) would correspond to HEFT upon using the translation of the parameters as in Table 1, except for differences due to the running in α_s , because no linearisation whatsoever in $1/\Lambda$ is present there.

3 Implementation and usage of the code within the Powheg-Box

3.1 Implementation of the NLO QCD corrections

Our implementation is similar to the NLO HEFT code `Powheg-Box-V2/ggHH`, which was presented in Refs. [40, 41] and is publicly available. For the virtual two-loop corrections, the NLO QCD corrections in the SM as calculated in Refs. [1, 2] have been used and extended to the SMEFT framework. The operator insertions have been included in a modular way, such that the different options described in the previous section can be calculated.

For the real emission part, the one-loop $2 \rightarrow 3$ matrix elements have been produced with `GoSam` [42, 43], based on a model which we generated in UFO format [44], specifying the anomalous couplings such that `GoSam` is able to calculate the different contributions according to the chosen truncation option. The existing interface [45] to `Powheg` [23–25] has been modified to hand over event parameters to `GoSam` in such a way that the factor α_s , which is included in the definition of the Higgs-gluon couplings in SMEFT, is evaluated at the correct energy scale. The renormalisation of the top-quark mass is performed in the on-shell scheme.

The code is built such that it splits the amplitude evaluation according to eq. (2.6), and the squared amplitude is calculated with truncation option (a), (b), (c) or (d) as defined by the user in the input card.

3.2 Usage within the Powheg-Box-V2

Usage of the program `ggHH_SMEFT` is similar to the HEFT public code `ggHH` [41], and both are provided within the POWHEG-BOX-V2 [25] under `User-Processes-V2`. The user defines the EFT parameters directly in the input card, of which we provide an example in `testrun/powheg.input-save`. The EFT mass scale is set by:

`Lambda=1.0`: the input value of the SMEFT heavy mass scale Λ (in TeV).

The value of the SMEFT coefficients in the Warsaw basis is set by the following keywords:

<code>CHbox</code> :	the Higgs kinetic term coefficient $C_{H,\Box}$,
<code>CHD</code> :	the Higgs kinetic term coefficient C_{HD} ,
<code>CH</code> :	the Higgs trilinear coupling term C_H ,
<code>CuH</code> :	the Higgs Yukawa coupling to up-type quarks term C_{uH} ,
<code>CHG</code> :	the effective coupling of gluons to Higgs bosons C_{HG} .

The input keyword `usesmeft` can be set to 0 or 1. When `usesmeft=1`, the above parameters for `CHbox`, `CHD`, `CH`, `CuH`, `CHG` are taken from the input card and translated internally to be used in the computation of the amplitude. If `usesmeft=0`, the values of the parameters `chhh`, `ct`, `ctt`, `cggh`, `cgghh` are used instead. If `usesmeft=1` is set, the values for the parameters `chhh`, `ct`, `ctt`, `cggh`, `cgghh` will be ignored.

Finally, the different SMEFT truncation options can be selected via the keyword `multiple-insertion`, where the options (a)–(d) in eq. (2.7) correspond to the values 0–3 of this flag. Apart from the above, the usage of the code is as described in [41] and in the `Docs` folder of the code. In particular, we remind the reader that the 2-loop grids for the virtual contributions have been generated with a *fixed* value of the Higgs and the top-quark masses, set respectively to $m_h = 125$ GeV and $m_t = 173$ GeV, and that these should not be changed (unless the user would like to calculate the leading order only). For the generation of full-fledged Monte-Carlo events an interface to `Pythia 8` [46, 47] and `Herwig 7` [48, 49] is provided that is identical to the one in `Powheg-Box-V2/ggHH`.

4 Results

Our results were produced for a centre-of-mass energy of $\sqrt{s} = 13$ TeV using the PDF4LHC15_nlo.30_pdfas [50] parton distribution functions interfaced to our code via LHAPDF [51], along with the corresponding value for α_s . The masses of the Higgs boson and the top quark have been fixed, as in the virtual amplitude, to $m_h = 125$ GeV,

$m_t = 173$ GeV and their widths have been set to zero. Jets are clustered with the anti- k_T algorithm [52] as implemented in the FastJet package [53, 54], with jet radius $R = 0.4$ and a minimum transverse momentum $p_{T,\min}^{\text{jet}} = 20$ GeV. We set the renormalisation and factorisation scales to $\mu_R = \mu_F = m_{hh}/2$.

4.1 Total cross sections

We consider three benchmark points, given in Table 2. Each of the benchmark points belongs to a characteristic m_{hh} shape cluster at NLO, as derived in Ref. [55].¹ The values for c_{gghh} have been modified in order to fulfil the SMEFT relation $c_{ggh} = 2c_{gghh}$. Here we consider three out of the seven shape types:

- benchmark 1: enhanced low m_{hh} region,
- benchmark 3: enhanced low m_{hh} and second local maximum above $m_{hh} \simeq 2m_t$,
- benchmark 6: close-by double peaks or shoulder left.

benchmark (* = modified)	c_{hhh}	c_t	c_{tt}	c_{ggh}	c_{gghh}	$C_{H,\text{kin}}$	C_H	C_{uH}	C_{HG}	Λ
SM	1	1	0	0	0	0	0	0	0	1 TeV
1*	5.105	1.1	0	0	0	4.95	-6.81	3.28	0	1 TeV
3*	2.21	1.05	$-\frac{1}{3}$	0.5	0.25*	13.5	2.64	12.6	0.0387	1 TeV
6*	-0.684	0.9	$-\frac{1}{6}$	0.5	0.25	0.561	3.80	2.20	0.0387	1 TeV

Table 2: Benchmark points used for the total cross sections and the distributions of the invariant mass of the Higgs-boson pair, cf. Table ?? and Figs. 2–4. The value of C_{HG} is determined using $\alpha_s(m_Z) = 0.118$.

In Table 3 we list total cross sections at 13 TeV for these three benchmark points for option (b) with $\Lambda = 1$ TeV, as well as the ratio to the SM cross section. The result for the total cross section with option (a) and the result for HEFT are also shown.

The squared modulus of the amplitude can be parametrised in terms of all possible coupling combinations appearing at fixed order, where the a_i have been defined as the

¹Here, we have updated a subset of the benchmark points identified in Ref. [55], performing the same clustering into seven characteristic shapes of the m_{hh} distribution with the help of unsupervised machine learning applied to HEFT results. However, we extracted central benchmarks under slightly tighter constraints to reflect more recent experimental measurements [56, 57], i.e. we used $0.83 \leq c_t \leq 1.17$ for all benchmarks, and additionally $|c_{tt}| < 0.05$ in the case of benchmark 1.

benchmark	$\sigma_{\text{NLO}}[\text{fb}]$ option (b)	K-factor option (b)	ratio to SM option (b)	$\sigma_{\text{NLO}}[\text{fb}]$ option (a)	$\sigma_{\text{NLO}}[\text{fb}]$ HEFT
SM	$27.94^{+13.7\%}_{-12.8\%}$	1.67	1	-	-
$\Lambda = 1 \text{ TeV}$					
1*	$71.95^{+20.1\%}_{-15.7\%}$	2.06	2.58	-57.64	91.62
3*	$68.69^{+9.4\%}_{-9.5\%}$	1.80	2.46	30.15	70.20
6*	$70.18^{+18.8\%}_{-15.5\%}$	1.83	2.51	50.82	87.9
$\Lambda = 2 \text{ TeV}$					
1*	$14.53^{+12.6\%}_{-12.2\%}$	1.62	0.52	6.44	-

Table 3: Total cross sections for Higgs-boson pair production at full NLO QCD for three benchmark points and truncation option (b) for $\Lambda = 1 \text{ TeV}$. The total cross sections for truncation option (a) are also given, in order to highlight the difference to the linearised case, as well as the values for HEFT. One can clearly see that truncation option (a) with $\Lambda = 1 \text{ TeV}$ is not a valid option for benchmark point 1*, leading to an unphysical cross section. The uncertainties are scale uncertainties based on 3-point scale variations. The values are the corrected values after the update of the code as described in Section 6.

coefficients of coupling combinations in HEFT at NLO QCD [11],

$$\begin{aligned}
|\mathcal{M}_{\text{BSM}}|^2 = & a_1 \cdot c_t^4 + a_2 \cdot c_{tt}^2 + a_3 \cdot c_t^2 c_{hhh}^2 + a_4 \cdot c_{ggh}^2 c_{hhh}^2 + a_5 \cdot c_{gghh}^2 + a_6 \cdot c_{tt} c_t^2 + a_7 \cdot c_t^3 c_{hhh} \\
& + a_8 \cdot c_{tt} c_t c_{hhh} + a_9 \cdot c_{tt} c_{ggh} c_{hhh} + a_{10} \cdot c_{tt} c_{gghh} + a_{11} \cdot c_t^2 c_{ggh} c_{hhh} + a_{12} \cdot c_t^2 c_{gghh} \\
& + a_{13} \cdot c_t c_{hhh}^2 c_{ggh} + a_{14} \cdot c_t c_{hhh} c_{gghh} + a_{15} \cdot c_{ggh} c_{hhh} c_{gghh} + a_{16} \cdot c_t^3 c_{ggh} \\
& + a_{17} \cdot c_t c_{tt} c_{ggh} + a_{18} \cdot c_t c_{ggh}^2 c_{hhh} + a_{19} \cdot c_t c_{ggh} c_{gghh} + a_{20} \cdot c_t^2 c_{ggh}^2 \\
& + a_{21} \cdot c_{tt} c_{ggh}^2 + a_{22} \cdot c_{ggh}^3 c_{hhh} + a_{23} \cdot c_{ggh}^2 c_{gghh} .
\end{aligned}$$

Truncation options (a) and (c) of eq. (2.7) are expansions at cross-section level, while (d) is the direct translation from HEFT to SMEFT. Therefore, for those cases the application of the translation of Table 1, including all terms at the desired order in $1/\Lambda$, is sufficient. For the truncation option (b), there are combinations which cannot be reconstructed from HEFT and therefore they have been calculated explicitly and implemented in analytic form.

In Fig. 1 we show heat maps illustrating the dependence of the cross section on the couplings C_H , C_{uH} (left) and C_H , $C_{H,\text{kin}}$ (right) with $\Lambda = 1 \text{ TeV}$ for the truncation

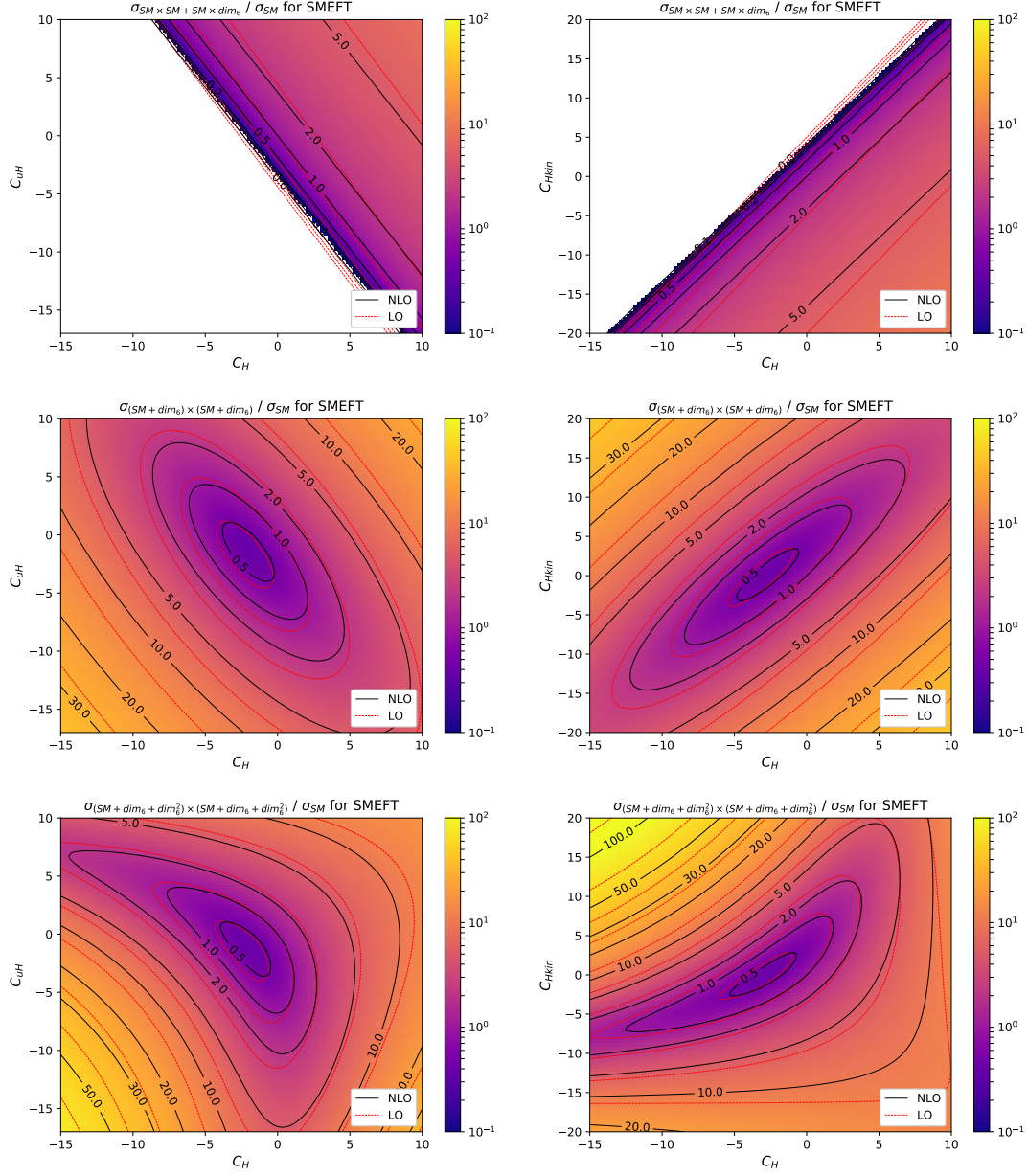


Figure 1: Heat maps showing the dependence of the cross section on the couplings C_H , C_{uH} (left) and C_H , $C_{H,\text{kin}}$ (right) with $\Lambda = 1$ TeV for different truncation options. Top: option (a) (linear dim-6), middle: option (b) (quadratic dim-6), bottom: option (d) (no linearisation in $1/\Lambda$). The white areas denote regions in parameter space where the corresponding cross section would be negative.

options (a) (linear dim-6, upper plots), (b) (quadratic dim-6, middle plots) and (d) (no linearisation, lower plots). We observe that the results for the total cross sections (normalised to the SM case) are substantially different between these options. The purely linear dim-6 contributions lead to negative cross sections over large parts of the parameter space, as manifested by the white areas in the top row of plots. This feature is not present at all when we consider the quadratic dim-6 truncation option. Furthermore, in the linear dim-6 case, we find completely flat directions in the considered parameter range for a combined variation of the respective Wilson coefficients. In the quadratic dim-6 case, option (b), iso-contours have an elliptic shape due to the quadratic terms in the cross section, while for option (d) the elliptic iso-contours are distorted due to higher terms in the polynomials in the Wilson coefficients.

4.2 Distribution of the Higgs-pair invariant mass m_{hh} : truncation effects

We now consider differential results and show the effect of the different truncation options on the distribution of the invariant mass m_{hh} of the Higgs-boson pair. We present results for the three benchmark points given in Table 2. We also show scale uncertainty bands for option (b) and the SM case, resulting from 3-point scale variations around the central scale $\mu_R = \mu_F = c \cdot m_{hh}/2$, with $c \in \{\frac{1}{2}, 1, 2\}$. For the SM case as well as for benchmark point 1 we have verified that 7-point scale variations lie within the 3-point scale uncertainty band.

The SMEFT results for benchmark points 1, 3 and 6 are shown in Figs. 2, 3 and 4, respectively, at $\Lambda = 1$ TeV (upper panels), $\Lambda = 2$ TeV (middle panels) and $\Lambda = 4$ TeV (lower panels), for the different truncation options (a) through (d), where the left (right) row shows LO (NLO) results. In the upper panels, we also display the HEFT results for the same benchmark point, with the translation given numerically in Table 2 for a value of $\Lambda = 1$ TeV. The dark blue curve corresponds to the linear dim-6 case, i.e. truncation option (a). As mentioned above, the negative differential cross-section values in the linear dim-6 case indicate that points in the coupling parameter space which are valid in HEFT can lead, upon naive translation of the Wilson coefficients, to parameter points for which the SMEFT expansion is not valid. The orange curve corresponds to the truncation option (b), where squared dim-6 contributions are taken into account. This choice, as well as option (c), leads to positive differential cross sections.²

²Nevertheless, one can question whether including an incomplete subset of $1/\Lambda^4$ contributions is theoretically well-defined (in particular whether such truncation options leave the theory gauge-invariant [19]). We take the view that these options can at least be useful in determining the magnitude of truncation uncertainties in $gg \rightarrow hh$. Furthermore, field redefinition ambiguities are expected to be suppressed in the $gg \rightarrow hh$ case as they enter via interference with a loop-induced SM amplitude [20].

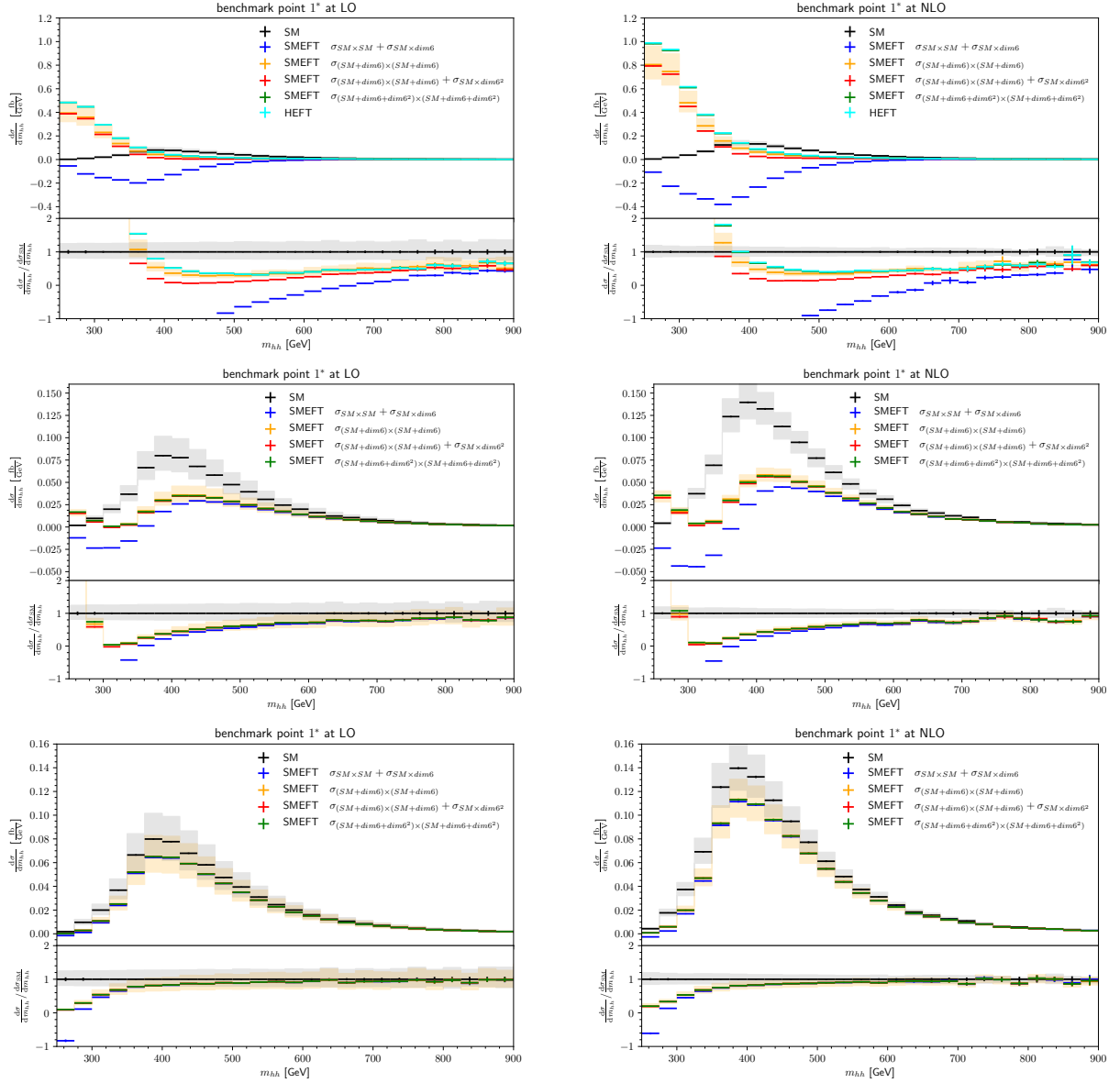


Figure 2: Differential cross sections for the invariant mass m_{hh} of the Higgs-boson pair for benchmark point 1 of Table 2. Top row: $\Lambda = 1$ TeV, middle row: $\Lambda = 2$ TeV, bottom row: $\Lambda = 4$ TeV. Left: LO, right: NLO. (All the subfigures show the corrected distributions after the update of the code, LO was not affected.)

For benchmark point 1, the characteristic shape in HEFT features an enhanced low- m_{hh} region. From Fig. 2 we see that this shape is not preserved in SMEFT as Λ increases. Disregarding the fully linearised option, which is simply not a valid option for this benchmark point, we see that the distribution develops a dip for $\Lambda = 2$ TeV; as the

other couplings are almost equal to the SM case, increasing Λ translates to decreasing the effective trilinear coupling, which becomes numerically close to the value of maximal destructive interference between box- and triangle-contributions. As the heavy scale is increased further to $\Lambda = 4$ TeV, the distribution approaches the SM shape. Note that for benchmark point 1, where c_{ggh} and c_{gghh} are zero, curves from option (d) (green) and HEFT (cyan) are identical at $\Lambda = 1$ TeV.

For benchmark point 3, the differences between the truncation options are very pronounced, see Fig. 3. The value of c_{hhh} is close to the value of maximal destructive interference between box- and triangle-type contributions when considering the cross section as a function of c_{hhh} alone, therefore delicate cancellations are likely to take place. Again, the m_{hh} -shape changes as Λ increases from 1 TeV to 2 TeV.

Furthermore, we observe that the contribution from the interference of double dimension-6 operator insertions with the SM, which appeared to be sub-dominant even for $\Lambda = 1$ TeV in the case of benchmark point 1, modifies the interference pattern considerably in the case of benchmark point 3, as can be seen by comparing truncation option (b) (orange) with option (c) (red), where the latter includes the double operator insertions interfered with the SM amplitude. While for $\Lambda = 1$ TeV the differences between the truncation options are large, benchmark point 3 shows a faster convergence to the SM shape as Λ increases. For $\Lambda = 4$ TeV, the scale uncertainty bands largely overlap with the SM uncertainty bands, except at very low and very high m_{hh} .

For benchmark point 6, the pattern of destructive interference between different parts of the amplitude (e.g. box- and triangle-type diagrams) in HEFT is similar to the one in the SM case. However, in SMEFT (taking the squared dim-6 level – option (b) – as reference), this interference pattern is modified, leading to a smaller cross section than in HEFT. Furthermore, the characteristic shape (see Fig. 4) is not preserved for any of the considered Λ values: in HEFT, the characteristic feature of benchmark 6 is a shoulder left. In SMEFT, this shoulder is absent (except for option (d) and $\Lambda = 1$ TeV, which corresponds to HEFT apart from the running of α_s).

Looking at the explicit values of the SMEFT coupling parameters in Table 2, stemming from the naive translation at $\Lambda = 1$ TeV between HEFT and SMEFT, it becomes clear that the parameters are too large for the SMEFT expansion to be valid. Therefore the large differences seen in the results at $\Lambda = 1$ TeV cannot be regarded as a truncation uncertainty. However, for $\Lambda = 2$ TeV these values are divided by a factor of 4 and for $\Lambda = 4$ TeV by a factor of 16, the latter case leading to perfectly valid SMEFT points for all three benchmarks. Except for benchmark 1, at $\Lambda = 4$ TeV, the scale uncertainty bands overlap with the SM case for almost all the m_{hh} range, so it seems that the parameter space where the SMEFT expansion is valid but still clearly distinguishable from the SM case (within NLO uncertainties) is rather small.

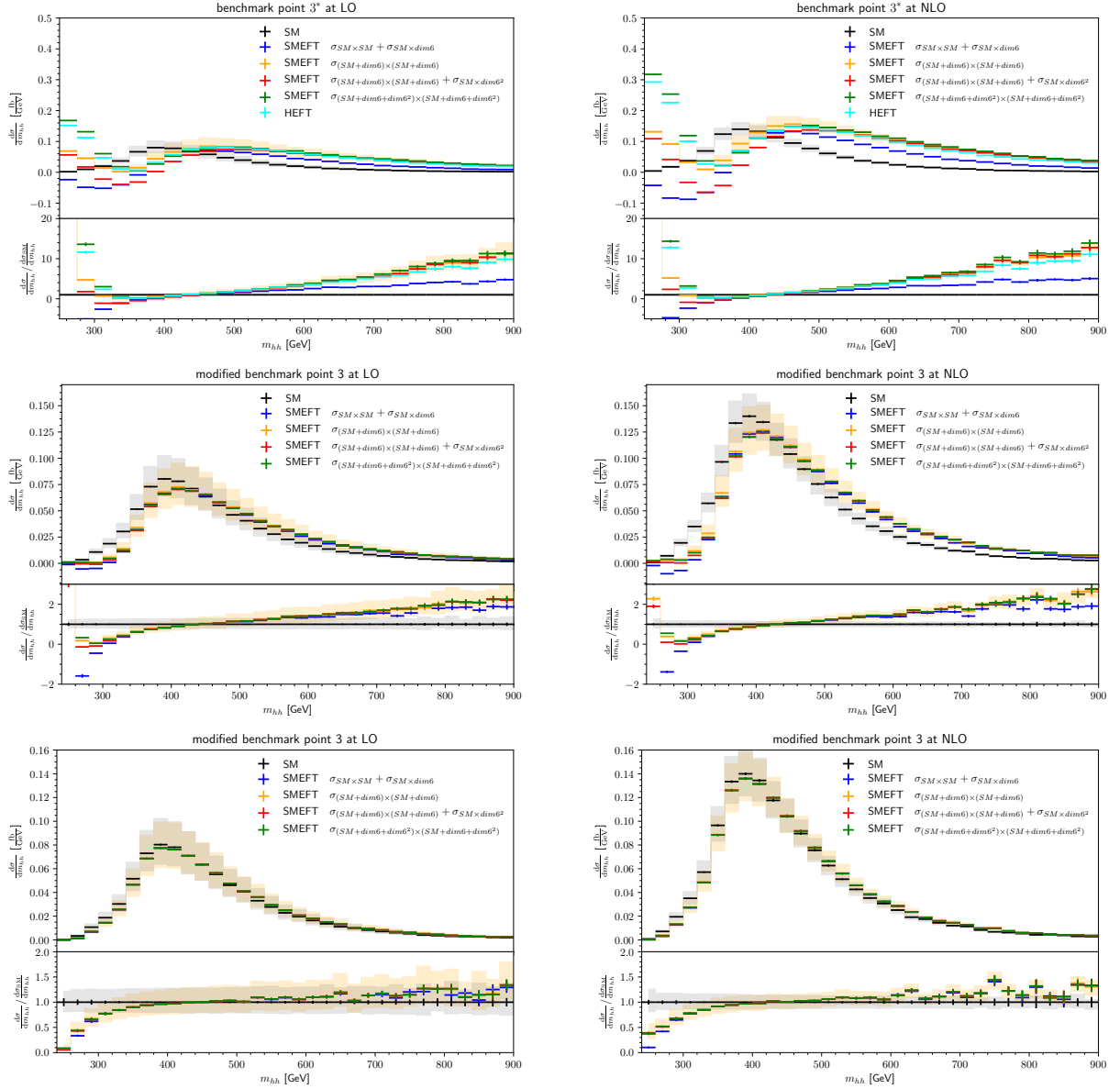


Figure 3: Differential cross sections for the invariant mass m_{hh} of the Higgs-boson pair for benchmark point 3 of Table 2. Top row: $\Lambda = 1$ TeV, middle row: $\Lambda = 2$ TeV, Bottom row: $\Lambda = 4$ TeV. Left: LO, right: NLO. (Plots resulting from the updated code, except for $\Lambda = 2$ TeV and $\Lambda = 4$ TeV at NLO, where the differences are at the sub-percent level.)

This implies that the variety of characteristic m_{hh} -shapes is diminished in SMEFT compared to HEFT.

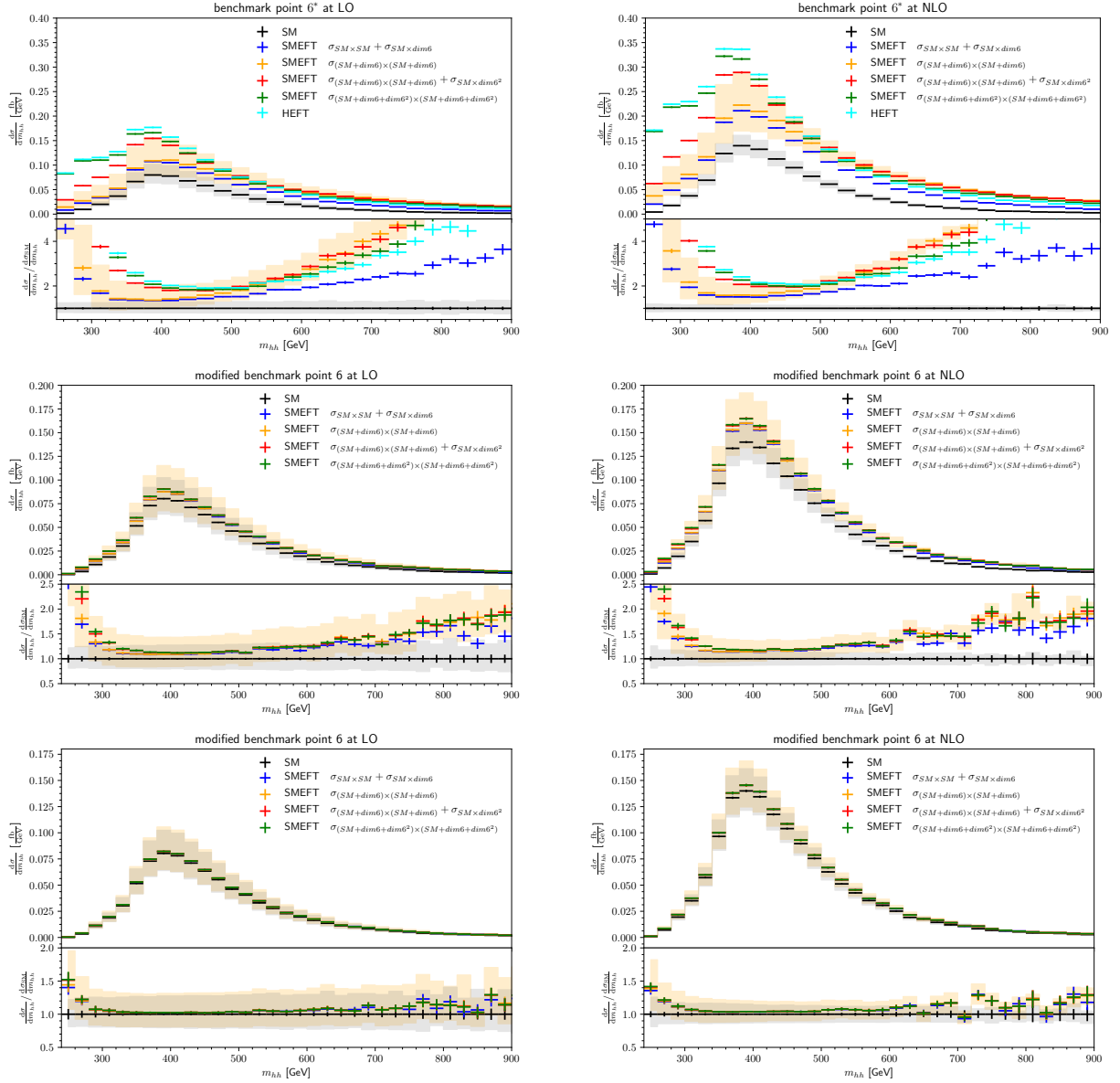


Figure 4: Differential cross sections for the invariant mass m_{hh} of the Higgs-boson pair for benchmark point 6 of Table 2. Top row: $\Lambda = 1$ TeV, middle row: $\Lambda = 2$ TeV, bottom row: $\Lambda = 4$ TeV. Left: LO, right: NLO. (Plots resulting from the updated code, except for $\Lambda = 2$ TeV and $\Lambda = 4$ TeV at NLO, where the differences are at the sub-percent level.)

5 Conclusions

We have presented the full NLO QCD corrections to Higgs-boson pair production in gluon fusion within the SMEFT framework. The corresponding matrix elements have been implemented in the `Powheg-Box-V2`³ in a flexible way, and allow the user to investigate the impact of different truncation options of the series in inverse powers of the new physics scale Λ . In particular, we have compared truncations in the inclusion of dimension-6 operators both at amplitude- as well as at cross-section level, and we have studied the effects of double operator insertions into single Feynman diagrams. We have also compared results from non-linear effective field theory (HEFT) to the different SMEFT truncation options for three benchmark points. While some of these truncation options only involve a subset of operators to be included in a consistent counting scheme, truncating the EFT expansion at the order $1/\Lambda^2$ either at cross-section level, or at amplitude level (where the latter option leads to $1/\Lambda^4$ -terms at cross-section level) are both options which are typically employed in fits to experimental data and which are useful for an estimation of truncation uncertainties.

It is well known that for values of the Wilson coefficients $C_i E^2/\Lambda^2 \ll 1$, the differences between the considered truncation options should be small for energies typical for LHC processes, i.e. $E \lesssim 1$ TeV. However, Higgs-boson pair production in gluon fusion is a process with delicate cancellations between different parts of the amplitude, such that small differences in the treatment of the Wilson coefficients can have a rather large effect, especially in differential distributions.

Furthermore, we have shown that a naive translation between HEFT and SMEFT Wilson coefficients, based on a comparison of terms at Lagrangian level, has to be done with great care (if at all). The two counting schemes rely on different assumptions, and for the SMEFT expansion to be valid, the values of $C_i E^2/\Lambda^2$ should be small. However, starting from a point in the space of anomalous couplings in HEFT that fulfils all the current constraints from measurements, after naive translation one easily ends up at values of C_i where the SMEFT expansion in $C_i E^2/\Lambda^2$ is not valid for $E \gtrsim m_{hh}$ and $\Lambda \simeq 1$ TeV, the latter being a value often used in the literature for this purpose.

We have illustrated the effects of such translations and of the different truncation options both at total cross-section level as well as for the m_{hh} distribution, at three benchmark points which are characteristic for a certain m_{hh} -shape in HEFT. In SMEFT, it is clear that the shape must change for fixed C_i as a function of Λ , as the SM shape is always approached for large values of Λ . At $\Lambda = 4$ TeV, two of the three

³The code can be downloaded from <https://powhegbox.mib.infn.it/> under User-Processes-V2/ggHH_SMEFT.

benchmark points lead to a m_{hh} distribution that is so close to the SM shape that it is indistinguishable from the SM within the NLO scale uncertainties.

6 Addendum

The current arXiv version contains the correction of a mistake that has been reported in the Erratum [https://doi.org/10.1007/JHEP10\(2023\)086](https://doi.org/10.1007/JHEP10(2023)086):

After comparison with the authors of Ref. [58], it turned out that the two-loop amplitude used in the original version of this manuscript was missing a term related to triangle-type two-loop diagrams, affecting the cases where the ratio between trilinear Higgs coupling c_{hhh} and Yukawa coupling modifier c_t is different from 1 (i.e. the Standard Model (SM) value), or when the effective coupling of a $t\bar{t}$ pair to a Higgs pair, c_{tt} , is nonzero. The SM results are unchanged. Therefore, benchmark points with a value of c_{hhh}/c_t or c_{tt} very different from the SM show the largest difference, which is up to 35% for benchmark point 1* in the kinematic range near $m_{hh} = 450$ GeV for truncation option (b), see Fig. 5. For the other truncation options and for HEFT the qualitative behaviour is similar. For benchmark points 3* and 6* the differences are below 10% and therefore within the scale uncertainties, as shown in Fig. 6.

The corrected figure for benchmark point 1* is shown in the main text in Fig. 2. For benchmark points 3* and 6* we show the corrected plots for $\Lambda = 1$ TeV in Figs. 3 and 4.

Acknowledgements

We are grateful to the authors of Ref. [58] for pointing us to the discrepancy with their result.

We also would like to thank Stephen Jones and Matthias Kerner for collaboration related to the $ggHH@NLO$ project and Gerhard Buchalla and Michael Trott for useful discussions. This research was supported by the Deutsche Forschungsgemeinschaft (DFG, German Research Foundation) under grant 396021762 - TRR 257. LS is supported by the Royal Society under grant number RP\R1\180112 and by Somerville College.

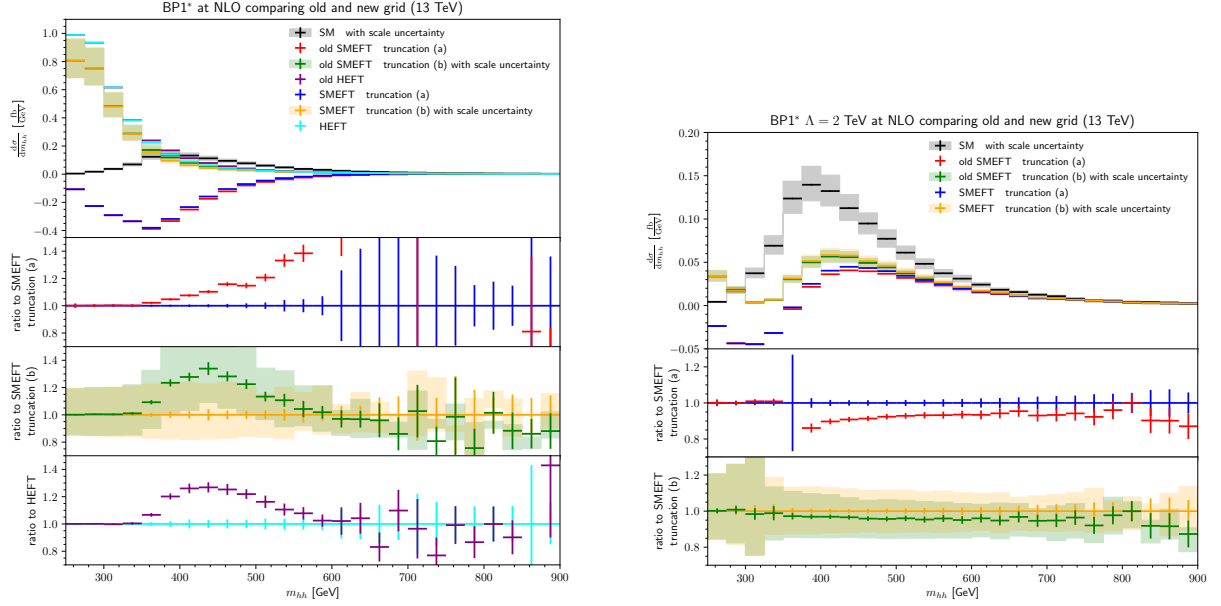


Figure 5: Comparison of old and new results for the cross sections differential in m_{hh} for benchmark point 1*, with $\Lambda = 1$ TeV (left) and $\Lambda = 2$ TeV (right), for truncation options (a) and (b). The HEFT distributions for benchmark point 1* are also included in the left plot. The lower panels show the truncation options separately and normalised to the corrected result (with 3-point scale variations for option (b)).

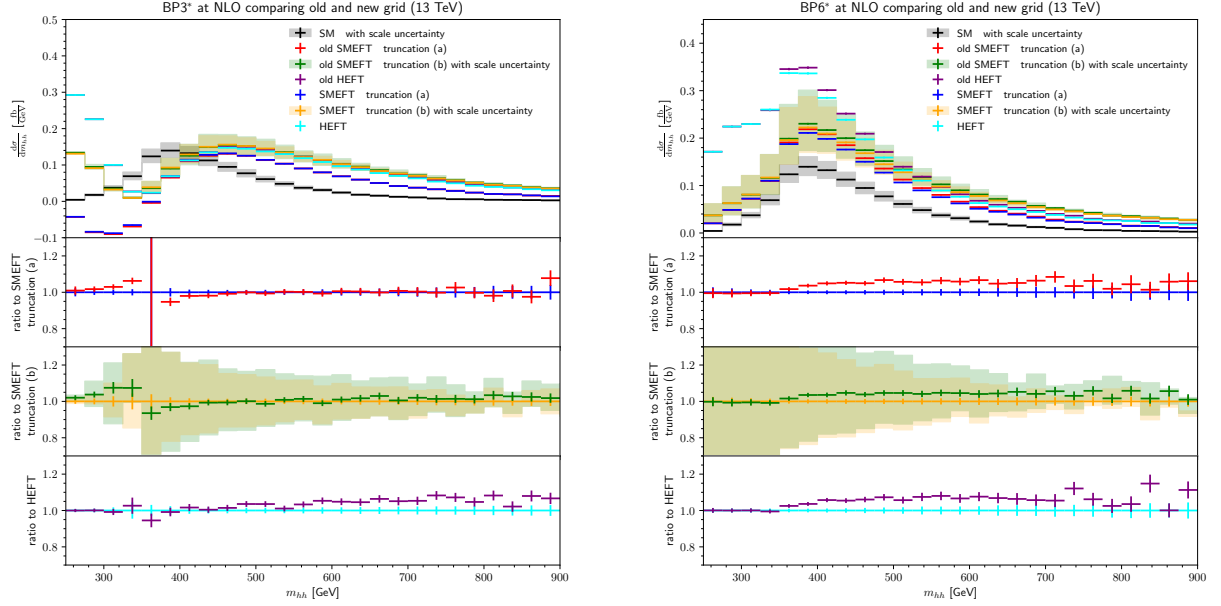


Figure 6: Comparison of old and new results for the cross sections differential in m_{hh} for benchmark points 3* and 6*, with $\Lambda = 1$ TeV and truncation options (a) and (b) and HEFT. The lower panels show the truncation options separately and normalised to the corrected result (with 3-point scale variations for option (b)).

References

- [1] S. Borowka, N. Greiner, G. Heinrich, S. P. Jones, M. Kerner, J. Schlenk et al., *Higgs Boson Pair Production in Gluon Fusion at Next-to-Leading Order with Full Top-Quark Mass Dependence*, *Phys. Rev. Lett.* **117** (2016) 012001 [[1604.06447](#)].
- [2] S. Borowka, N. Greiner, G. Heinrich, S. P. Jones, M. Kerner, J. Schlenk et al., *Full top quark mass dependence in Higgs boson pair production at NLO*, *JHEP* **10** (2016) 107 [[1608.04798](#)].
- [3] J. Baglio, F. Campanario, S. Glaus, M. Mühlleitner, M. Spira and J. Streicher, *Gluon fusion into Higgs pairs at NLO QCD and the top mass scheme*, *Eur. Phys. J. C* **79** (2019) 459 [[1811.05692](#)].
- [4] J. Baglio, F. Campanario, S. Glaus, M. Mühlleitner, J. Ronca, M. Spira et al., *Higgs-Pair Production via Gluon Fusion at Hadron Colliders: NLO QCD Corrections*, *JHEP* **04** (2020) 181 [[2003.03227](#)].
- [5] M. Grazzini, G. Heinrich, S. Jones, S. Kallweit, M. Kerner, J. M. Lindert et al., *Higgs boson pair production at NNLO with top quark mass effects*, *JHEP* **05** (2018) 059 [[1803.02463](#)].
- [6] L.-B. Chen, H. T. Li, H.-S. Shao and J. Wang, *Higgs boson pair production via gluon fusion at N^3LO in QCD*, *Phys. Lett. B* **803** (2020) 135292 [[1909.06808](#)].
- [7] L.-B. Chen, H. T. Li, H.-S. Shao and J. Wang, *The gluon-fusion production of Higgs boson pair: N^3LO QCD corrections and top-quark mass effects*, *JHEP* **03** (2020) 072 [[1912.13001](#)].
- [8] J. Baglio, F. Campanario, S. Glaus, M. Mühlleitner, J. Ronca and M. Spira, *$gg \rightarrow HH$: Combined uncertainties*, *Phys. Rev. D* **103** (2021) 056002 [[2008.11626](#)].
- [9] R. Gröber, M. Mühlleitner, M. Spira and J. Streicher, *NLO QCD Corrections to Higgs Pair Production including Dimension-6 Operators*, *JHEP* **09** (2015) 092 [[1504.06577](#)].
- [10] R. Gröber, M. Mühlleitner and M. Spira, *Higgs Pair Production at NLO QCD for CP-violating Higgs Sectors*, *Nucl. Phys. B* **925** (2017) 1 [[1705.05314](#)].
- [11] G. Buchalla, M. Capozzi, A. Celis, G. Heinrich and L. Scyboz, *Higgs boson pair production in non-linear Effective Field Theory with full m_t -dependence at NLO QCD*, *JHEP* **09** (2018) 057 [[1806.05162](#)].
- [12] D. de Florian, I. Fabre and J. Mazzitelli, *Higgs boson pair production at NNLO in QCD including dimension 6 operators*, *JHEP* **10** (2017) 215 [[1704.05700](#)].
- [13] D. de Florian, I. Fabre, G. Heinrich, J. Mazzitelli and L. Scyboz, *Anomalous couplings in Higgs-boson pair production at approximate NNLO QCD*, *JHEP* **09** (2021) 161 [[2106.14050](#)].

- [14] A. Biekötter, J. Brehmer and T. Plehn, *Extending the limits of Higgs effective theory*, *Phys. Rev. D* **94** (2016) 055032 [[1602.05202](#)].
- [15] I. Brivio et al., *Truncation, validity, uncertainties*, [2201.04974](#).
- [16] S. Dawson, S. Homiller and M. Sullivan, *Impact of dimension-eight SMEFT contributions: A case study*, *Phys. Rev. D* **104** (2021) 115013 [[2110.06929](#)].
- [17] J. Lang, S. Liebler, H. Schäfer-Siebert and D. Zeppenfeld, *Effective field theory versus UV-complete model: vector boson scattering as a case study*, *Eur. Phys. J. C* **81** (2021) 659 [[2103.16517](#)].
- [18] SMEFT collaboration, J. J. Ethier, G. Magni, F. Maltoni, L. Mantani, E. R. Nocera, J. Rojo et al., *Combined SMEFT interpretation of Higgs, diboson, and top quark data from the LHC*, *JHEP* **11** (2021) 089 [[2105.00006](#)].
- [19] M. Trott, *Methodology for theory uncertainties in the standard model effective field theory*, *Phys. Rev. D* **104** (2021) 095023 [[2106.13794](#)].
- [20] A. Martin and M. Trott, *ggh variations*, *Phys. Rev. D* **105** (2022) 076004 [[2109.05595](#)].
- [21] M. Battaglia, M. Grazzini, M. Spira and M. Wiesemann, *Sensitivity to BSM effects in the Higgs p_T spectrum within SMEFT*, *JHEP* **11** (2021) 173 [[2109.02987](#)].
- [22] R. Aoude, E. Madge, F. Maltoni and L. Mantani, *Quantum SMEFT tomography: top quark pair production at the LHC*, [2203.05619](#).
- [23] P. Nason, *A New method for combining NLO QCD with shower Monte Carlo algorithms*, *JHEP* **11** (2004) 040 [[hep-ph/0409146](#)].
- [24] S. Frixione, P. Nason and C. Oleari, *Matching NLO QCD computations with Parton Shower simulations: the POWHEG method*, *JHEP* **11** (2007) 070 [[0709.2092](#)].
- [25] S. Alioli, P. Nason, C. Oleari and E. Re, *A general framework for implementing NLO calculations in shower Monte Carlo programs: the POWHEG BOX*, *JHEP* **06** (2010) 043 [[1002.2581](#)].
- [26] W. Buchmüller and D. Wyler, *Effective Lagrangian Analysis of New Interactions and Flavor Conservation*, *Nucl. Phys. B* **268** (1986) 621.
- [27] B. Grzadkowski, M. Iskrzynski, M. Misiak and J. Rosiek, *Dimension-Six Terms in the Standard Model Lagrangian*, *JHEP* **10** (2010) 085 [[1008.4884](#)].
- [28] I. Brivio and M. Trott, *The Standard Model as an Effective Field Theory*, *Phys. Rept.* **793** (2019) 1 [[1706.08945](#)].
- [29] G. Buchalla, G. Heinrich, C. Müller-Saldaña and F. Pandler, *Loop counting matters in SMEFT*, [2204.11808](#).

- [30] C. Arzt, M. B. Einhorn and J. Wudka, *Patterns of deviation from the standard model*, *Nucl. Phys. B* **433** (1995) 41 [[hep-ph/9405214](#)].
- [31] F. Feruglio, *The Chiral approach to the electroweak interactions*, *Int. J. Mod. Phys. A* **8** (1993) 4937 [[hep-ph/9301281](#)].
- [32] C. P. Burgess, J. Matias and M. Pospelov, *A Higgs or not a Higgs? What to do if you discover a new scalar particle*, *Int. J. Mod. Phys. A* **17** (2002) 1841 [[hep-ph/9912459](#)].
- [33] B. Grinstein and M. Trott, *A Higgs-Higgs bound state due to new physics at a TeV*, *Phys. Rev. D* **76** (2007) 073002 [[0704.1505](#)].
- [34] R. Contino, C. Grojean, M. Moretti, F. Piccinini and R. Rattazzi, *Strong Double Higgs Production at the LHC*, *JHEP* **05** (2010) 089 [[1002.1011](#)].
- [35] R. Alonso, M. B. Gavela, L. Merlo, S. Rigolin and J. Yepes, *The Effective Chiral Lagrangian for a Light Dynamical "Higgs Particle"*, *Phys. Lett. B* **722** (2013) 330 [[1212.3305](#)].
- [36] G. Buchalla, O. Catà and C. Krause, *Complete Electroweak Chiral Lagrangian with a Light Higgs at NLO*, *Nucl. Phys. B* **880** (2014) 552 [[1307.5017](#)].
- [37] S. Weinberg, *Phenomenological Lagrangians*, *Physica A* **96** (1979) 327.
- [38] G. Buchalla, O. Catà and C. Krause, *On the Power Counting in Effective Field Theories*, *Phys. Lett. B* **731** (2014) 80 [[1312.5624](#)].
- [39] C. G. Krause, *Higgs Effective Field Theories - Systematics and Applications*, Ph.D. thesis, Munich U., 2016. [1610.08537](#). 10.5282/edoc.19873.
- [40] G. Heinrich, S. P. Jones, M. Kerner, G. Luisoni and L. Scyboz, *Probing the trilinear Higgs boson coupling in di-Higgs production at NLO QCD including parton shower effects*, *JHEP* **06** (2019) 066 [[1903.08137](#)].
- [41] G. Heinrich, S. P. Jones, M. Kerner and L. Scyboz, *A non-linear EFT description of $gg \rightarrow HH$ at NLO interfaced to POWHEG*, *JHEP* **10** (2020) 021 [[2006.16877](#)].
- [42] G. Cullen, N. Greiner, G. Heinrich, G. Luisoni, P. Mastrolia, G. Ossola et al., *Automated One-Loop Calculations with GoSam*, *Eur. Phys. J. C* **72** (2012) 1889 [[1111.2034](#)].
- [43] G. Cullen et al., *GOSAM-2.0: a tool for automated one-loop calculations within the Standard Model and beyond*, *Eur. Phys. J. C* **74** (2014) 3001 [[1404.7096](#)].
- [44] C. Degrande, C. Duhr, B. Fuks, D. Grellscheid, O. Mattelaer and T. Reiter, *UFO - The Universal FeynRules Output*, *Comput. Phys. Commun.* **183** (2012) 1201 [[1108.2040](#)].
- [45] G. Luisoni, P. Nason, C. Oleari and F. Tramontano, *$HW^\pm/HZ + 0$ and 1 jet at NLO with the POWHEG BOX interfaced to GoSam and their merging within MiNLO*, *JHEP* **10** (2013) 083 [[1306.2542](#)].

- [46] T. Sjöstrand and P. Z. Skands, *Transverse-momentum-ordered showers and interleaved multiple interactions*, *Eur. Phys. J.* **C39** (2005) 129 [[hep-ph/0408302](#)].
- [47] T. Sjöstrand, S. Ask, J. R. Christiansen, R. Corke, N. Desai, P. Ilten et al., *An Introduction to PYTHIA 8.2*, *Comput. Phys. Commun.* **191** (2015) 159 [[1410.3012](#)].
- [48] G. Marchesini and B. R. Webber, *Monte Carlo Simulation of General Hard Processes with Coherent QCD Radiation*, *Nucl. Phys.* **B310** (1988) 461.
- [49] J. Bellm et al., *Herwig 7.0/Herwig++ 3.0 release note*, *Eur. Phys. J. C* **76** (2016) 196 [[1512.01178](#)].
- [50] J. Butterworth et al., *PDF4LHC recommendations for LHC Run II*, *J. Phys.* **G43** (2016) 023001 [[1510.03865](#)].
- [51] A. Buckley, J. Ferrando, S. Lloyd, K. Nordström, B. Page, M. Rüfenacht et al., *LHAPDF6: parton density access in the LHC precision era*, *Eur. Phys. J.* **C75** (2015) 132 [[1412.7420](#)].
- [52] M. Cacciari, G. P. Salam and G. Soyez, *The anti- k_T jet clustering algorithm*, *JHEP* **04** (2008) 063 [[0802.1189](#)].
- [53] M. Cacciari and G. P. Salam, *Dispelling the N^3 myth for the k_t jet-finder*, *Phys.Lett.* **B641** (2006) 57 [[hep-ph/0512210](#)].
- [54] M. Cacciari, G. P. Salam and G. Soyez, *FastJet User Manual*, *Eur.Phys.J.* **C72** (2012) 1896 [[1111.6097](#)].
- [55] M. Capozzi and G. Heinrich, *Exploring anomalous couplings in Higgs boson pair production through shape analysis*, *JHEP* **03** (2020) 091 [[1908.08923](#)].
- [56] CMS collaboration, *Combined Higgs boson production and decay measurements with up to 137 fb^{-1} of proton-proton collision data at $\sqrt{s} = 13\text{ TeV}$* , tech. rep., 2020.
- [57] ATLAS collaboration, *Combined measurements of Higgs boson production and decay using up to 139 fb^{-1} of proton-proton collision data at $\sqrt{s} = 13\text{ TeV}$ collected with the ATLAS experiment*, tech. rep., 2021.
- [58] E. Bagnaschi, G. Degrandi and R. Gröber, *Higgs boson pair production at NLO in the POWHEG approach and the top quark mass uncertainties*, [2309.10525](#).